Proceedings of the ASME 2018 Pressure Vessels and Piping Conference
PVP2018
July 15-20, 2018, Prague, Czech Republic

PVP2018-84484

STUDY OF MODE I-II MIXED CRACK PROPAGATION IN ELECTROFUSION JOINT OF POLYETHYLENE PIPE

Yue Zhang, Jianfeng Shi, Jinyang Zheng
Institute of Process Equipment
(Zhejiang University, Hangzhou, P. R. China)
Zheda Road, Hangzhou 310027
Zhejiang, P. R. China.

ABSTRACT

Electrofusion joint plays an important role in connecting polyethylene (PE) pipe. In our previous study, penetrating crack failure through the fitting with an angle of about 70° was observed, and axial stress was found to be an important factor in the crack propagation. In this paper, experiments were carried out to study the crack propagation phenomena of the electrofusion joint of PE pipe. Digital Image Correlation (DIC) method was used to measure the displacement on specimen's surface, as well as full-field strain distribution, based on which the J-integral of the crack tip was calculated. Besides, a finite element numerical simulation was conducted, and its accuracy was verified by experimental J-integral value. Through combination of experimental observations and finite element method, the phenomenon that the angle between crack propagation direction and tube axial is about 70° is detailed analysed. By comparison and analysis of the testing results, critical J-integral value during crack propagation is determined. Furthermore, critical J-integral value of crack propagation in electrofusion joint is predicted.

INTRODUCTION

Pipe joint is the weak link in the safety of pipeline system. At present, electric welding is widely used in plastic pipes and plastic composite pipes. According to statistics of Plastic Pipe Data Collection in America, most of the failure accidents of polyethylene pipe occurred in joint[1]. Welding inevitably causes defects in welding joint. We applied phased array ultrasonic technique (PAUT) and managed to detect all typical flaws in electrofusion (EF) joint and butt fusion (BF) joint. Typical flaws have been catagorized into four types, such as metal wire dislocation, void, poor fusion interface and cold welding[2]. Shi et al.[3] concluded failure modes of EF joints into three kinds: fusion interface failure, crack failure along the plane of the metal wire, and crack failure through electrofusion fitting wall. Specifically, the third failure mode shows the characteristics of slow crack growth (SCG). It's caused by the inclusion defects of fusion interface which is connected to the cold region. These defects will produce stress concentration at the end of the cold region, and will slowly propagate through the fitting wall with an angle of about 70 ° under long term hydrostatic test. SCG is the main failure mode of PE pipes under long-term low stress condition, whose initiation of crack may pass through several decades but may fracture in a very short period of time. Study on crack propagation phenomena basically focuses on three aspects, which is crack initiation, crack propagation direction and crack arrest.

The J-integral, proposed by Rice in 1968[4], is defined as a path independent integral around the crack tip, it's a parameter to characterize average strength of the stress and strain field under elastoplastic condition, as known as energy release rate. One of the great advantage of the use of J-integral is the use of the measured displacement fields at a distance reasonably far from the crack tip[5], and its integral value is proved to be independent of path, as well as the critical value J_{IC} is independent of specimen's type and dimension. Rosegren and Hutchinson did approximate analysis on plastic stress field of plane crack tip with the use of J-integral respectively, and obtained the stress and strain field of the crack tip[6].

Till now, various crack propagation criterions have been proposed. Typically, existing crack propagation criterions have two catagories, which are stress criterion and energy criterion. The former contains maximum circumferential tensile stress criterion[7] and maximum shear stress criterion; the latter contains strain energy density factor criterion[8], distortion

*corresponding author: shijianfeng@zju.edu.cn

energy criterion[9], and energy release rate criterion[10]. However, most of the criterions are suitable for brittle materials, only energy release rate energy is suitable for viscoelastic materials. Besides, geometric criterion such as crack tip opening angle (CTOA), crack tip opening displacement (CTOD), and CTOD-time curve criterion have also been used to both brittle and ductile materials, as well as viscoelastic material. Considering the viscoelasticity of PE material, energy release rate criterion, also known as J-integral criterion was used to study the crack propagation in this paper.

In order to calculate J-integral with experimental approach, displacement field as well as strain field near the crack tip is needed. Digital Image Correlation (DIC) technique is an advanced measurement combining digital image processing and numerical analysis. As a new and advanced optical measurement method, DIC has been successfully applied to many fields in scientific research and engineering practice[11]-[12]. Comparing with traditional mearsurements, DIC method has advantages of: 1) capable of non-contact measurements; 2) capable of dynamic full field measurements; 3) high accuracy and the distribution of measured objects can be known clearly; 4) low requirement on the environment, available for abnormal environment such as noise and high temperture.

As an approach to evaluating fracture parameters, lots of studies have been made with DIC technique. Sahlaabadi M. et al.[13] used a combined experimental finite element method (FEM) to determine J-integral and Q parameter in central cracked HDPE, relation between J-integral and Q parameter, as well as hydrostatic stress around the crack was obtained. M. Mokhtarishirazabad et al.[14] studied the influence of parameters such as magnification factor, the position of the images with respect to the crack tip and size of the subset used in DIC, with the calculation of stress intensity factor, they found that accuracy of stress intensity factor (SIF) can be affected not only by subset size in DIC considered number of Williams' series, but also by the size and position of area of interest (AOI). Besides, various methods for evaluating J-integral utilising photomechanics techniques have been developed. Wang et al.[15] evaluated J-integeral of crack in elastoplastic material using DIC, they used Hooke's law to calculate stress, and J-integral and fracture toughness J_C are evaluated directly from strain fields around crack tip. Soneda et al.[16] used dot patterns and image processing to obtain the displacement fields, J-integral was evaluated with FEM. Becker et al.[17] also used a finite element model to process the experimental data to evaluate J-integral. However their methods are limited to elastic deformation, which is not of feasibility when material exists large-scale yielding[18]. Han G. et al.[19] evaluated J-integral and COD near crack tip of elastoplastic material. Similar hybrid method [20][21] conducted by other researchers all adopted similar approach which is to calculate stresses with method of elastoplastic FEM.

Many researchers have studied the fracture parameters with experimental approaches though, there's still few reports on viscoelastic material as PE. PE exhibits great decrease in modulus with time increasing and large deformation depending on strain rate, which leads to the great difficulty in evaluating the stress in the vicinity of crack tip. In our previous study, we proposed a constitutive model for large deformation behavior of PE considering strain rate effect[22], and a relaxation constitutive model to describe the long-time stress and strain relation. In this paper, DIC method was adopted to measure the displacement distribution on specimen's surface, and J-integral was evaluated by MATLAB and simulated by ABAQUS with the large deformation constitutive model and relaxation constitutive model. Through combination of these two methods, the critical J-integral criterion of crack propagation was evaluated.

EXPERIMENTAL METHODOLOGY

Digital Image Correlation Technique

Basic Principle

DIC is a widespread optical technique to perform full field strain measurement utilising sequential images taken by single camera for 2D measurement or more cameras for 3D measurements. Displacement and strain are calculated by matching the position relation of corresponding point, line segment and area of the measured object before and after deformation. Fig. 1ure 1 shows the relationship of dot in subset before and after deformation. P(x_0, y_0) is the center of the subset, after deformation, P moves to P'(x_0', y_0') with displacement of (u, v), then the first-order derivative and second derivative is:

$$\frac{\partial u}{\partial x},\frac{\partial u}{\partial y},\frac{\partial^2 u}{\partial x^2},\frac{\partial^2 v}{\partial y^2},\frac{\partial^2 u}{\partial x\partial y},\frac{\partial v}{\partial x},\frac{\partial v}{\partial y},\frac{\partial^2 v}{\partial x^2},\frac{\partial^2 v}{\partial y^2},\frac{\partial^2 v}{\partial x\partial y}$$

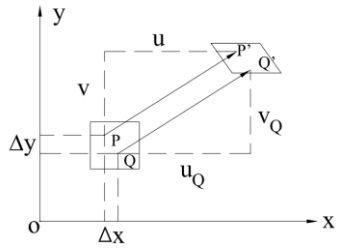

Fig. 1 Correspondence between subsets before and after deformation

Q(x, y) is a random dot in the subset, there is:

$$PQ = \Delta x + \Delta y \tag{1}$$

When Q moves to Q'(x', y') with displacement of (u_Q, v_Q), it can be seen from Fig. 1 that after deformation, the coordinates of P' and Q' can be expressed as:

$$\begin{aligned} x_0' &= x_0 + u \\ y_0' &= y_0 + v \end{aligned} \tag{2}$$

$$\begin{aligned} x' &= x + u_Q \\ y' &= y + v_Q \end{aligned} \tag{3}$$

When DIC technique processes with speckle image, subregion as initial sample image before deformation for DIC caluclation is needed, whose gray value is $f(x, y)$, then program will search image in the corresponding selected area of speckle pattern after deformation, whose gray value is $g(x', y')$. Once the gray values are obtained, correlation of undeformed sample

image and deformed target image is established, it reflects the similarity degree of the two images. According to statistics, correlation C is defined as:

$$C = \frac{\sum f(x,y)g(x',y')}{\sqrt{\sum f^2(x,y)g^2(x',y')}} \tag{4}$$

where C=1 means the two subregion is completely correlated, and C=0 means the two subregion is not correlated.

Displacement field measurement is based on the measurement of the pixel displacement. Before measurement analysis is conducted, calculated section needs to be pre-selected, scattered speckles in the area are the default calculation points. According to continuity deformation hypothesis, displacement information of current point is calculated as initial value the next measurement point. However, when there are discontinuities such as cracks, voids or other discontinuity deformation in digital images, errors will occur, and calculation of subsequent points will be further affected. Furthermore, strain field measurement is based on numerical differentiation:

$$\varepsilon_x = \frac{\partial u}{\partial x}, \varepsilon_y = \frac{\partial v}{\partial y}, \varepsilon_{xy} = \frac{1}{2}(\frac{\partial u}{\partial y} + \frac{\partial v}{\partial x}) \tag{5}$$

Error analysis

Measurement accuracy of the DIC system is influenced by imaging system, loading system and software related algorithms.

1) Speckle quality: DIC calculation is carried out through speckle image, hence, speckle quality will directly affect the results of calculation. Speckle distribution should be uniform in black and white, particularly, large spots shouldn't be found in important computing areas;

2) Distance and parallel between lens and specimen: basic principle of 2D DIC requires flat images, therefore specimen surface should be parallel to camera lens, so as to ensure the parallel of the CCD sensor and specimen. It's reported that a non parallel angle of less than 5 degrees will cause a displacement deviation of 0.01 pixels[23]. Besides, distance between camera and specimen determines the field of view, as a result, subset size of calculating region should be reasonably small to ensure calculation accuracy.

3) Noise and vibration: noise and vibartion will generate randomly during the process of image acquisition. Consequently, experimental site should be selected in a relatively quiet enviromonent to minimize the interference.

Evaluating J-integral Based on DIC Displacement Fields

The J-integral is defined as a path independent integral to characterize the stress and strain singularity in area of interest (AOI) around the crack tip.

$$J = \int_\Gamma W dy - \vec{T}\frac{\partial \vec{u}}{\partial x} ds \tag{6}$$

where Γ is any counterclockwise path around the crack tip, W is the total strain energy density, $\vec{T}$ is the traction energy, ds is the increment of Γ, and $\vec{u}$ is the displacement vector.

Conventionally, a rectangluar path is selected when evaluating the J-integral with experimental measurement. In order to simplify the calculation, integral discretization is needed. A total integral path is divided into five lines as shown in Fig. 2, marked with 1~5. Points A and F are the starting point and ending point of the integral path, respectively, and points B, C, D, E are the inflection points.

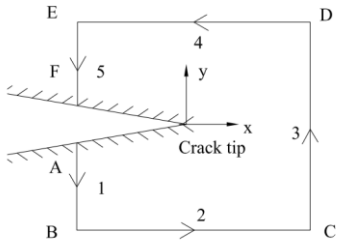

Fig. 2 Integral path of J-integral

The next step is to discretize the integral path, such as:

$$J = \int_{1,3,5} W dy - \int_{1,2,3,4,5} T_i \frac{\partial u_i}{\partial x} ds \tag{7}$$

Total strain energy density is calculated from:

$$W = \int_0^{\varepsilon_{ij}} \sigma_{ij} d\varepsilon_{ij} = \frac{1}{2}\sigma_{ij}\varepsilon_{ij} = \frac{1}{2}(\sigma_x\varepsilon_x + \sigma_y\varepsilon_y + \tau_{xy}\gamma_{xy}) \tag{8}$$

where σ_{ij} is the stress tensor and ε_{ij} is the strain tensor. Under the condition of plane stress, W is calculated as Eq. (8), where σ_x and σ_y are the stress in x and y direction respectively, and ε_x and ε_y are the stress in x and y direction respectively, τ_{xy} and γ_{xy} are the shear stress and shear strain respectively.

Numbers of 200 stress and strain data as well as their components obtained from the full field displacement with DIC were extracted for each integrating path, and J-integral was calculated by MATLAB.

Constitutive Model Used in MATLAB

Viscoelasticity of PE determines its large deformation behavior. According to Zhong S et al.[22], constitutive relation for PE is described as:

$$\sigma_t(\varepsilon_t)\big|_{\dot{\varepsilon}_t^*} = C(\varepsilon_t)\cdot\dot{\varepsilon}_t^{*m(\varepsilon_t)} \tag{9}$$

where σ_t and ε_t are the current stress and current strain respectively, $\dot{\varepsilon}_t^*$ is the strain rate, $C(\varepsilon_t)$ and $m(\varepsilon_t)$ are function of current strain respectively.

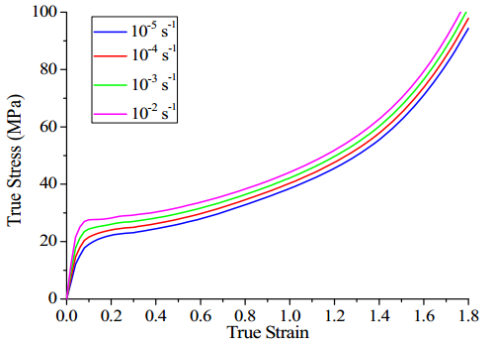

Fig. 3 Sress-strain curves at constant true strain rate[22]

From figure above, one can know that while strain is smaller than 0.1, coefficient m and C can be regarded as constant, therefore, stress-strain relation can be considered as linear. However, Eq. 9 was obtained from tensile tests at different strain

rates, the relaxation phenomenon with time is not considered. Therefore a relaxation constitutive model is needed, for it reflects the material's mechanical behavior of experiment conducted in this paper (under constant load). Relaxation model with a Prony series representation is shown as:

$$E(t) = E_\infty + \sum_{i=1}^{N} E_i e^{-t/\tau_i} \tag{10}$$

where $E(t)$ is the relaxation modulus, E_∞ is the equilibrium modulus, E_i and τ_i are the modulus and relaxation time respectively, and N is the item number of series. Parameters are obtained from relaxation tests of 8 MPa at temperatures ranging from 25℃~95℃, with the utilization of Williams-Landel-Ferry fuction, as shown in Table 1[24].

Table 1 Parameters of Prony sereis at 25℃

E_∞	E_1	E_2	E_3	E_4
110.89	68.04	42.72	32.20	46.96
	τ_1	τ_2	τ_3	τ_4
	0.0057	0.0567	0.5756	9.4870

EXPERIMENTAL PROCEDURE

A penetrating crack failure through the fitting with an angle of 70° caused by fusion interface inclusion defect was observed by Shi[1], which shows characteristic of SCG failure. In order to study crack propagation process induced by this type of defect, experiments were conducted in this section. Experiments were conducted on a specimen which was extracted and machined from EF joints of PE80-DN110-SDR11. Defects were made by binding a layer of Teflon tape on the surface of PE pipe to be welded to reduce the length of welding fusion face. Figure 4 illustrates the specimen geometry and dimensions. And Fig. 5 detailedly demonstrates the location of teflon tape.

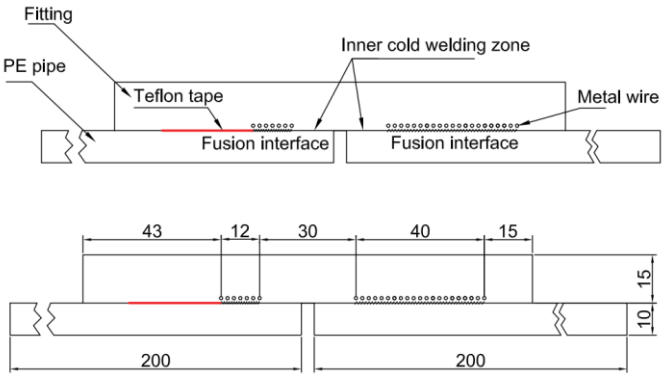

Fig. 4 Specimen dimension and structural annotation

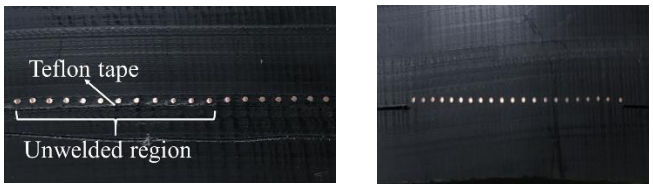

(a)defect in fusion interface (b) normal interface

Fig. 5 Cross-section of welding region

RESULTS AND DISCUSSION

Experimental Observation

Creep test of 8 MPa at 25℃ was conducted on specimen. Stress was applied on the end of the pipe, so a tensile stress as well as a bending moment will act on the fitting. It's obverved a crack in the inner cold welding zone would firstly appeare once the load was applied, as shown in Fig. 6. And a rectangular damage zone along an angle of about 70° with the axial direction of the pipe was also observed. It's known that heating metal wires destroy the continuity of the PE material inside the EF joint, resulting in the structrual discontinuity, which is equivalent to introducing initial defects into the material, and lead to stress concentration. Besides, the bonding force between the metal wire and PE material is very weak, therefore, once the stress reaches a certain value, crack will soon appear around the metal wire.

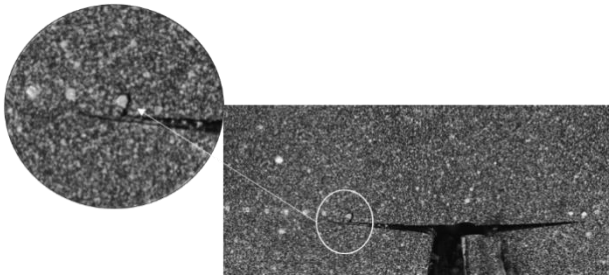

Fig. 6 Specimen morphology (0.01h)

Figure 7 demonstrates the specimen morphology after the experiment lasted 1.75 h. it can be seen from the figure that with the energy accumulates and releases, crack in the inner cold welding zone propagates along the right side of damage zone. At the same time, a whistle-like hole appears at the first metal wire location in the fusion region (R1). Similarly, there appears a rectangular damage zone along an angle of 75° with the axial direction of the pipe. As stated above, bonding force between metal wire and material is weak, therefore, with the deformation of pipe getting larger, a hole emerges between the metal wire and pipe material.

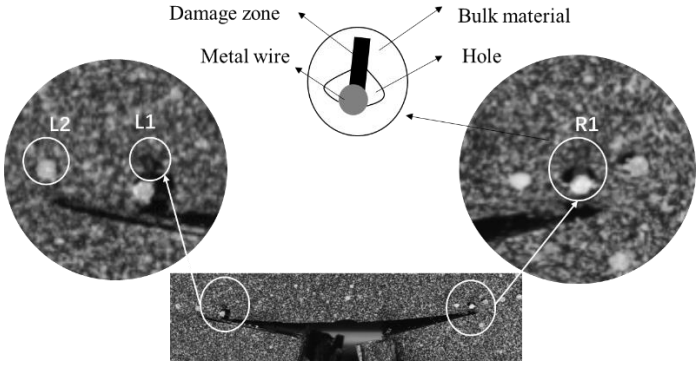

Fig. 7 Specimen morphology (1.75h)

As illustrated in Fig. 8, with the increase of experimental time, crack locates at the inner cold welding region continues growing until crack tip reaches the end of damage zone. Besides, another whistle-like hole begin to emerge in the fusion region(L2). As for the whistle-like hole in the right circle, it continues growing larger, but the damage zone seems stay

unchanged. This is because the deformation during 1.75 h ~ 47.2 h is concentrated in the lower part of the metal wire (see where the arrow locates). At the same time, two whistle-like holes (R2, R3) emerge on the right side of the existing hole. It can be extrapolated that with the increase of experimental time, once the material under the first metal wire breaks, crack will propagate along the left side of rectangular damage zone, which reproduces the crack behavior of the crack in the left circle. It's noteworthy that the inconsistent number of cracks/holes on both sides of the fitting comes from the different length of the fusion region on both sides, resulting in asymmetry deformation of specimen.

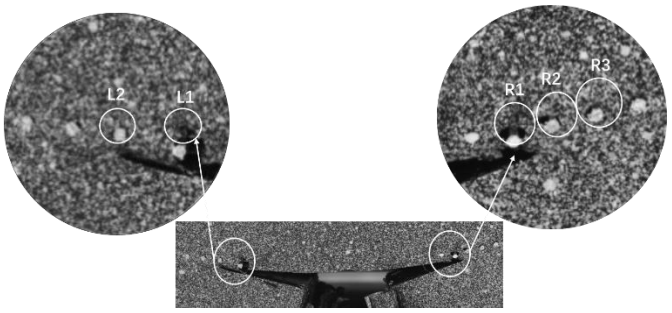

Fig. 8 Specimen morphology (47.2h)

Direction of Crack Propagation

Numerical simulation

From experimental observation above, we can notice that the crack direction around metal wire is about 70° with axial direction, so a numerical analysis was conducted in this subsection to study the direction of crack propagation.

Geometric Model and Boundary Conditions

Finite element (FE) model was created and analyzed with ABAQUS software. Geometric model adopted in this subsection is shown as Fig. 9. The model is built in ANSYS, and then imported into ABAQUS. In order to simplify calculation and for qualitatively analysis, PE material is assumed to be elastic material, metal wire and unwelded region of fitting's left side was removed. Actually, when a crack locating at inner welding zone extends through the fitting, two steps are necessary: 1) crack extends to metal wire; 2) stress concentrates at metal wire, then initial crack initiates and gradually extends through the fitting. However, the first step is not our study focus. Therefore our simulation in this subsection starts from the second step. As shown in Fig. 9, a crack is preset in the first metal wire locating in intersection of inner cold welding region and welded region. C3D8R element is employed for the whole model. And 6 constraints is set at the right end, and 5 constraints is set at the left end except for tensile direction. Tensile stress is 8 MPa.

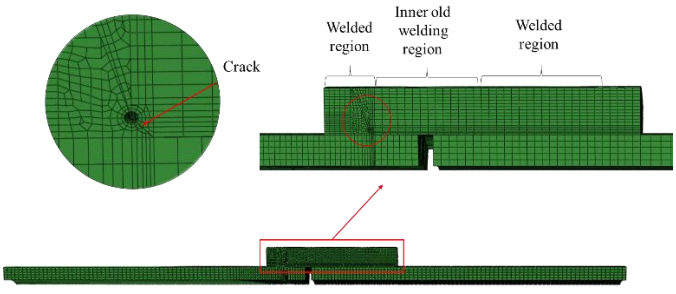

Fig. 9 Finite element model

Numerical results

Numerical results are shown in Fig. 10. Both the maximum Von-mises stress and the Tresca stress concentrates at about 105° around metal wire. It's known that stress concentration is easily produced at maximum stress, resulting in the condition of initiation of crack. So initial crack will produce at about 105° with x direction, which is also 75° with tensile direction, corresonding to experimental observation.

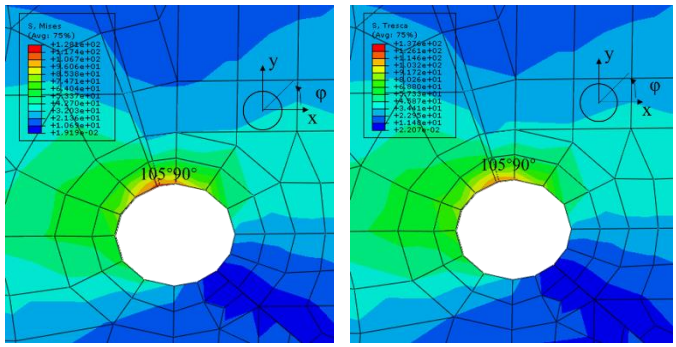

(a) Von-Mises stress (b) Tresca stress

Fig. 10 Stress distribution around metal wire

Crack propagation direction is analyzed with fracture mechanics theory. Figure 11 shows the force analysis schematic diagram, axial force, shear force and bending force caused by axial force both act on the fitting. If unwelded part of cold welding region is considered as a crack, for inner cold welding region, structure is mainly subjected to shear stress, so a mode II crack may produce; while for inner cold welding region, structure is mainly subjected to nomal stress, but due to crack position deviation or asymmetry load, a mode I-II crack may produces.

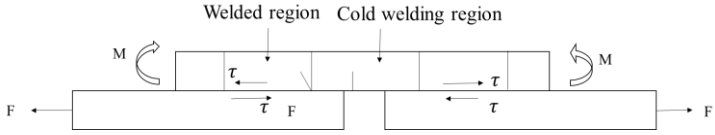

Fig. 11 Schematic diagram of force

The experimental observation shows that a crack of about 70° produces around metal wire. And the numerical result shows that stress concentration at 75° with tensile diretion around metal wire creates a precondition for crack initiation. Therefore, a precrack of 75° is set at where the maximum stress locates, shown in Fig. 12, to study the crack propagation.

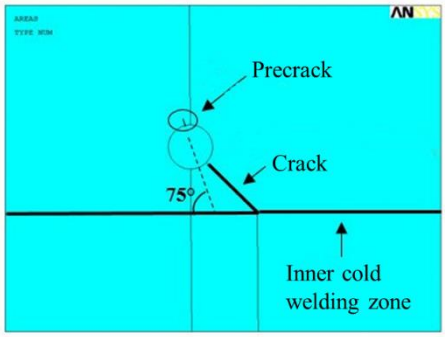

Fig. 12 Crack propagation analytical model

According to linear fracture mechanics, crack propagation caused by the asymmetry of crack direction belongs to mixed mode I-II. The stress field of crack tip is described as:

$$\begin{cases} \sigma_{rr} = \dfrac{K_I}{2\sqrt{2\pi r}}\cos\dfrac{\theta}{2}(3-\cos\theta) + \dfrac{K_{II}}{2\sqrt{2\pi r}}\sin\dfrac{\theta}{2}(3\cos\theta-1) \\ \sigma_{\theta\theta} = \dfrac{K_I}{2\sqrt{2\pi r}}\cos\dfrac{\theta}{2}(1+\cos\theta) - \dfrac{3K_{II}}{2\sqrt{2\pi r}}\cos\dfrac{\theta}{2}\sin\dfrac{\theta}{2} \\ \sigma_{r\theta} = \dfrac{K_I}{2\sqrt{2\pi r}}\cos\dfrac{\theta}{2}\sin\theta + \dfrac{K_{II}}{2\sqrt{2\pi r}}\cos\dfrac{\theta}{2}(3\cos\theta-1) \end{cases} \tag{11}$$

where K_I and K_{II} is the stress intensity factor of mode I and II respectively, MPa·mm$^{1/2}$; r and θ are polar coordinates; σ_{rr}, $\sigma_{r\theta}$, and $\sigma_{\theta\theta}$ are radial stress, shear stress and circumferential stress respectively, MPa.

According to maximum circumferential stress criterion, crack extends in radius direction with maximum circumferential stress and shear stress of zero, such as:

$$\frac{\partial\sigma_{\theta\theta}(K_I, K_{II}, \theta)}{\partial\theta} = 0 \tag{12}$$

The solution can be obtained as:

$$\theta_0 = 2\tan^{-1}\left[\frac{1}{4}\left(\frac{K_I}{K_{II}} \pm \sqrt{\left(\frac{K_I}{K_{II}}\right)^2 + 8}\right)\right] \tag{13}$$

Table 2 indicates the variation among stress intensity factor ratio K_{II}/K_I, and crack length. During the process of crack extention, K_I is much bigger than K_{II}, so crack propagation is controlled by mode I crack, hence, the crack will propagate along the path of 75° with tensile direction.

Table 2 Stress intensity factor ratio-carck length relation

Crack length(mm)	2	3	4	5	6
K_{II}/K_I	0.003	0.030	0.056	0.079	0.132

Experimental results

The DIC analysis was conducted with a normalized-sum-of –squared-differences correlation algorithm with subset size of 23 pixels(1.15mm), step size of 7 pixel (0.35mm). Figure 13 shows an example of the principal strain angle fields obtained for 7MPa load. It can be seen that the data points around the crack faces and crack tips (near the metal wires) were excluded from the analysis automatically to avoid high noise resulting from abrupt changes in displacement.

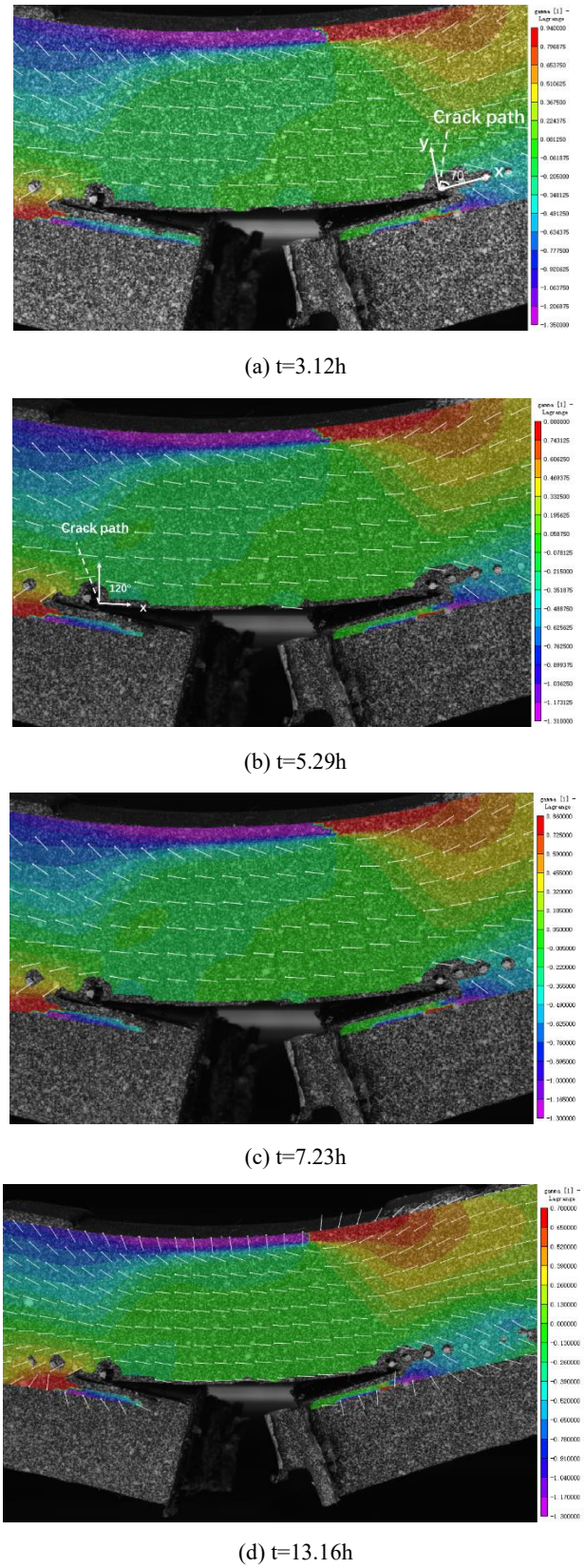

(a) t=3.12h

(b) t=5.29h

(c) t=7.23h

(d) t=13.16h

Fig. 13 Maximum principal streamlines

Arrow flows in Fig. 13 intuitively demonstrate the streamlines of maximum principal strain, each arrow indicates

the direction of current maximum principal strain, so crack will extend perpendicular to the arrow. From the four figures, one can see that direction of maximum principal strain located at the front of the crack barely changes, and Fig. 13 (a) shows an crack path angle of 70° , while Fig. 13 (b) shows an angle of 60° with axial direction. Fitting edge at the left crack is broken, and about 3/4 of the bulk material around the metal wire is stripped off, resulting in large deformation and rotation of crack. Even if there are some differences between the two figures, the reason why the crack extention is about 70° with axial direction still can be reasonably explained intuitively.

J-integeral Calculation

Experimental calculation

J-integral calculation was carried out with specimen with a 2mm crack in the inner cold welding zone. This crack is perpendicular to tensile direction. It's analysed that this crack is caused by defects in bulk material. To calculate the J-integral values from the measured DIC displacement field, three different rectangular integral paths were defined symmetrically about horizontal axis to represent the area of interest (AOI) as shown in Fig. 14. It should be noticed that the AOI is inverse correlated with plastic zone, which means that, in order to study AOI's influence on the estimating accuracy of J-integral value, the plastic zone will reversibly increase. The principle of choosing integral path is the path should be large enough to include the plastic region.

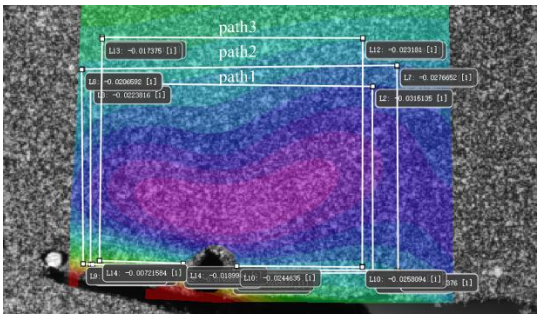

Fig. 14 crack path used for J-integeral analysis

Figure 15 shows the the relation between J-integral value and testing time. It's found that although the dispersion of data is large, their tendency is consistent. J-integeral value increases dramatically over time, and reach its peak at 15 N/mm averagely when testing time is 4 h, then decreased and bottomed out at about 5 N/mm. Figure 16 describes the crack opening displacement (COD)'s variation over testing time. COD ascends appreciably in the first 4 h, and then grows slowly.

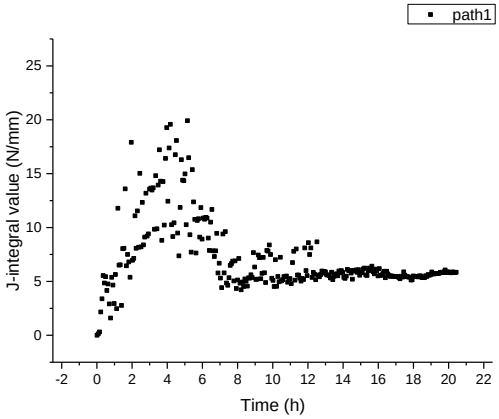

Fig. 15 J-integral value-time curve of path-1

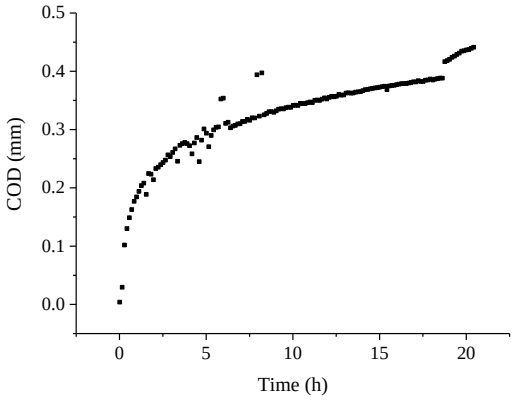

Fig. 16 COD-time curve of path-1

Meanwhile, change regulation between J value and COD can be seen clearly from Fig. 17. Curves were obtained by taking average 18 points to reduce data size and make even spaced time using Origin software, as a consequence, the variation trend of curve can be seen clearly. J value reaches the top (15 ± 2 KN/m) slowly as COD increases at about 0.28mm, and then falls as the crack angle continues opening. It indicates that when crack opens to critical value of 0.28mm, J value reaches the maximum value and crack propagates.

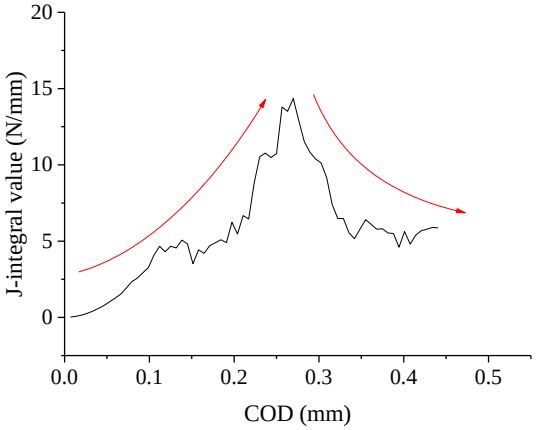

Fig. 17 J-integral value- COD curve of path-1

Comparisons among J values obtained from different paths

are shown in Fig. 18. Curves wereprocessed as Fig. 20. Tendency of J value is consistent in different integral paths. Their maximum value is about 15 N/mm, 15 N/mm, 10 N/mm respectively. Theoretically J-integral value should be independent of integral path, while in practical calculation, integral path is unable to form a closed loop, for DIC is unable to obtain the deformation near the crack tip and crack face due to distortion and uncontinuous displacement, resulting in different J-integeral value with different integral path.

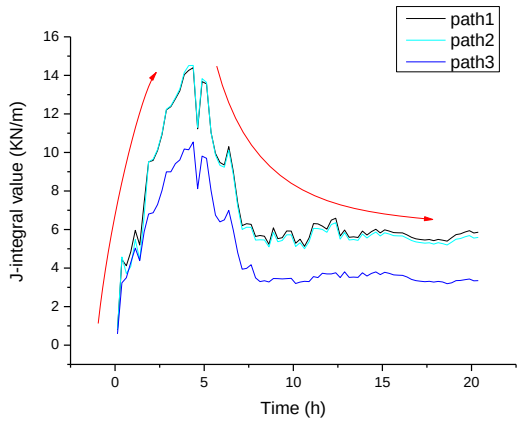

Fig. 18 J-integral value comparison among different paths

Numerical results

Contour integeral method was used to calculate the J-integral value in this subsection.

Geometric Model and Boundary Conditions

FE model size was refered to experimental specimen. It's noteworthy that metal wires and unwelded parts were removed to reduce computational calculation and get better convergence. Figure 19 demonstrates the FE model and a crack is set in the inner cold welding zone. C3D8R element was employed for the whole model. 6 constraints is set at the right end, and 5 constraints is set at the left end except for tensile direction. Tensile stress is 8 MPa.

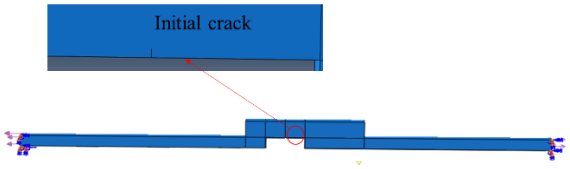

Fig. 19 FE model and initial crack settlement

In this paper, contour integral was adopted to calculate J-integral value around crack tip. 15 contours was defined in history output to observe J value's variation versus different integral paths and determine appropriate J value.

Material Property

Material in this subsection is defined as viscoelastic at time domain with Prony series. Basic form of Prony series in ABAQUS is:

$$G(t)=G_\infty+\sum_{i=1}^{N}G_i e^{-t/\tau_i}=G_0(g_\infty+\sum_{i=1}^{N}g_i e^{-t/\tau_i})$$
$$K(t)=K_\infty+\sum_{i=1}^{N}K_i e^{-t/\tau_i}=K_0(k_\infty+\sum_{i=1}^{N}k_i e^{-t/\tau_i}) \quad (14)$$

where $G(t)$ is the relaxation shear modulus, G_∞ is the equilibrium shear modulus, G_i is the shear modulus at different time, G_0 is the instantaneous shear modulus, g_∞ is the relative equilibrium shear modulus and g_i is the relative shear modulus; $K(t)$ is the relaxation bulk modulus, K_∞ is the equilibrium bulk modulus, K_i is the bulk modulus at different time, K_0 is the instantaneous bulk modulus, k_∞ is the relative equilibrium bulk modulus and k_i is the relative bulk modulus. Define:

$$G_0=G(t=0)=G_\infty+\sum_{i=1}^{N}G_i, g_\infty=\frac{G_\infty}{G_0}, g_i=\frac{G_i}{G_0}$$
$$K_0=K(t=0)=K_\infty+\sum_{i=1}^{N}K_i, k_\infty=\frac{K_\infty}{K_0}, k_i=\frac{K_i}{K_0} \quad (15)$$

where corresponding G and K are obtained correspondingly from Table 1, calculated with Possion ratio ν=0.45:

$$G=\frac{E}{2(1+\nu)}, K=\frac{E}{3(1-2\nu)}$$

Numerical result

Contour integral of static crack was conducted utilizing ABAQUS to verify the accuracy of J-integral value obtained from DIC method. Figure 20 shows different contour integral values in different paths. J values vary considerably from 15 N/mm~ 17 N/mm. In ABAQUS, contour number equals to the number of layers of meshes around crack tip. It's known that crack tip exists singularity, so stress around crack tip is not calculated accurately. So integral path is defined a distance far from crack tip.

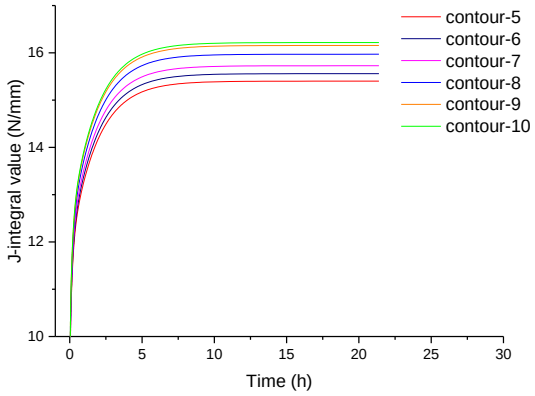

Fig. 20 Numerial J-integral values in different paths

As aforementioned, J-integral value around crack tip obtained from numerical calculation range from 15 N/mm ~17 N/mm, which is in consistency with average experimental value. And it takes about 5 hours to reach the maximum J value, which is equivalent to the experimental result. Good agreement between experiment and simulation proves accuracy of the experimental results.

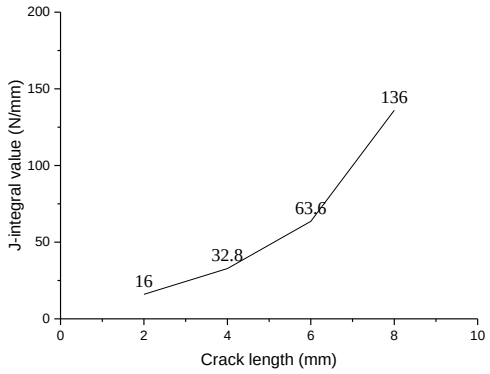

Fig. 21 J-integral value- initial crack length prediction

Figure 21 shows a J-integral value prediction along initial pre-defined crack length. It indicates that under constant tensile stress, crack fracture energy grows with crack length. It's easy to understand the trend. With the increase of crack length, the effective loading area decreases, then resulting in a sharp increase of stress and strain in the vicinity of crack, hence the increase of J value. Notice that the simulation is carried out with static crack, which means the crack cannot extend, so the J value won't descend after it reach its maximum. While for actually dynamic cracking, if crack length is 2 mm, cracking will occur when J value reaches about 15 N/mm after about 5 hours, then J value descends as energy accumulated around crack tip is released, then with the new crack length, J value increases over time to reach its new critical value, crack extends forward again. Repeatedly, the staged crack expansion is captured.

CONCLUSIONS

1) The full-field displacement and strain distribution obtained from DIC test and analysis proved to be effective in crack propagation analysis in EF joint.

2) In welded region, mode II crack of 70° with tensile direction initiates around metal wire, and crack propagation is predominantly controlled by mode I; in inner cold welding region, mode I-II crack may occur due to initial defects in bulk material. Crack propagation in EF joint is predominanly mode I crack.

3) Based on the DIC results, when J-integral value reaches to 15 N/mm, crack begins to propagate. The J-integral value obtained from simulation corresponds well with experimental results.

ACKNOWLEDGMENTS

The authors gratefully acknowledge the financial support from the National Natural Science Foundation of China (Project No.51575480) and the Fundamental Research Funds for the Central Universities (Grant No. 2017FZA4012), and also would like to thank Ms. Ping Qiu and Ms. Sijia Zhong for their guidance with DIC system, and Xianpeng Chen from Zhejiang Qingfa Industrial Co. for providing materials.

REFERENCES

[1] Shi J. Formation mechanism, inspection and safety assessment of electrofusion joint cantaining cold welding defect. Zhejiang University, China, 2011.

[2] Hou D, Guo W, Zheng J. A method of automatic defect recognition for phased array ultrasonic inspection of polythene electro-fusion joints. ASME 2015 Pressure Vessels and Piping Conference, Boston, USA, 2015, V5T-V9T.

[3] Shi J, Guo W, Shi J, et al. Development of non-destructive testing and safety assessment of polyethylene and composite pipes[J]. Ciesc Journal. 13, 756-764.

[4] J.R. Rice, A path independent integral and the approximate analysis of strain concentration by notches and cracks, J. Appl. Mech. 35 (1968) 379–386.

[5] Gonzáles G L G, González J A O, Castro J T P, et al. A J-integral approach using digital image correlation for evaluating stress intensity factors in fatigue cracks with closure effects[J]. Theoretical & Applied Fracture Mechanics, 2017.

[6] Jiang Yuchuan. The research of J* integral in elastic-plastic fracture mechanics and fracture criterion for mixed mode crack propagation. Sichuan University.2004.

[7] Erdogan F, Sih G C. On the Crack Extension in Plates Under Plane Loading and Transverse Shear[J]. Journal of Basic Engineering, 1963, 85(4):527.

[8] Sih G C. Energy-density concept in fracture mechanics [J]. Engineering Fracture Mechanics, 1973, 5(4):1037-1040.

[9] Jiang Yu-chuan, Wang Qi-zhi.Distortion Energy Criterion for mixed mode crack propagation[J]. Journal of Sichuan University(Engineering Science Edition), 2004, 36(3):20-23.

[10] Nuismer R J. An energy release rate criterion for mixed mode fracture[J]. International Journal of Fracture, 1975, 11(2):245-250.

[11] Huang Y H. Optical strain gauge vs. traditional strain gauges for concrete elastiticity modulus determination[J]. Optik-International Journal for Light and Electron Optics, 2009, 120(3):2.

[12] Pan B, Xie H M, Hua T, et al. Measurement of coefficient of thermal expansion of films using digital image

[13] Sahlabadi M, Valiollahi A, Konh B, et al. Evaluating J - integral and Q parameter in high-density polyethylene using a combined experimental finite element method: Evaluating J-integral and Q parameter in HDPE[J]. Fatigue & Fracture of Engineering Materials & Structures, 2016.

[14] Mokhtarishirazabad M, Lopez-Crespo P, Moreno B, et al. Evaluation of crack-tip fields from DIC data: A parametric study[J]. International Journal of Fatigue, 2016, 89:11-19.

[15] Wang, H.-W., Kang, Y.-L., Zhang, Z.-E. and Qin, Q.-H. Size effect on the fracture toughness of metallic foil. Int. J. Fract. 2003,123–3/4, 177–185.

[16] Soneda, N., Yoshimura, S. and Yagawa, G. Measurement of J-integral using stress and strain fields near a crack tip: an application of the computer picture processing (in Japanese), J. Soc. Mater. Sci. 1989, Jpn. 37–419, 957–963.

[17] Becker, T. H., Mostafavi, M., Tait, R. B. and Marrow, T. J. An approach to calculate the J-integral by digital image correlation displacement field measurement. Fatigue Fract.

Eng. Mater. Struct. 2012, 35–10, 971–984.
[18] S. Yoneyama, S. Arikawa, S. Kusayanagi, and K. Hazumi. Evaluating J-integral from displacement fields measured by digital image correlation. Strain. 2014, 50, 147-160.
[19] Han, G., Sutton, M. A. and Chao, Y.-J. A study of stationary crack-tip deformation fields in thin sheets by computer vision. Exp. Mech. 1994, 34–2, 125–140.
[20] Hareesh, T. V. and Chaing, F. P. Integrated experimental-finite element approach for studying elastoplastic crack-tip fields. Eng. Fract. Mech. 1988, 31–3, 451–461.
[21] Sivaneri, N. T., Xie, Y. P. and Kang, B. S.-J. Elastic–plastic crack-tip-field numerical analysis integrated with moiré interferometry. Int. J. Fract., 1991, 49–4, 291–303.
[22] Zhong S, Shi J, Zheng J. Study on Constitutive Modeling for Large Deformation Behavior of Polyethylene Considering Strain Rate Effect[C]. ASME 2013 Pressure Vessels and Piping Conference. 2013:V06BT06A048.
[23] Meng L., Jin G., Yao X. Errors caused by misalignment of the optical camera axis and the object surface in the DSCM. Tsinghua Univ.,2006, 46:1930-1932.
[24] Zhang Y., Luo X., Shi J. Viscoelastic and damage model of polyethylene pipe material for slow crack growth analysis. ASME 2017 Pressure Vessels and Piping Conference. 2017: V03BT03A045.